JPE 17-3-21

https://doi.org/10.6113/JPE.2017.17.3.788
ISSN(Print): 1598-2092 / ISSN(Online): 2093-4718

Single-phase Cascaded H-bridge Multilevel Active Power Filters in AC Electric Railway Systems

Liran Wu* and Mingli Wu†

*,†School of Electrical Engineering, Beijing Jiaotong University, Beijing, China

Abstract

The power quality of AC electric railways has become an issue worthy of more and more concern. Many active compensators based on power converters have been proposed, but with complex transformers or coupled branches. This paper presents a single-phase cascaded H-bridge multilevel active power filter (APF), which can directly connect to the 27.5-kV power supplies to deal with power quality problems. According to field measured data, the load characteristics are analyzed, and the system configuration and control system are designed based on the load characteristic analysis. Finally, simulation and experimental results verify the effectiveness of the proposed APF system, considering some problems such as the supply voltage fluctuations and transient inrush currents in AC electric railway systems.

Key words: AC electric railway, Active power filter, Cascaded H-bridge, Power quality

I. INTRODUCTION

The single-phase AC 25 kV industrial frequency supply has been widely adopted for long-distance railways in many countries. Electric locomotives and EMUs (electric multiple units), operating on the AC electric railway, are typical nonlinear dynamics and time varying loads with the phase-controlled thyristor converters or PWM converters to feed the traction motors [1], [2]. Due to their inherent electrical characteristics, electric vehicles introduce reactive power and harmonic distortion problems into traction power supply systems [3]. As the amount of rail traffic increases, the issue of power quality is becoming increasingly critical [4].

The reactive power, produced by the electric vehicles, leads to low power factors and supply voltage drops. It may generate undesired power loss and cause damage to the entire system [5]. In addition, massive harmonics cause overheating and noise of transformers, malfunctions of circuit breakers, communications line failure, and distorted pantograph voltage waveforms [3], which limits the performance of electric vehicles. Significant resonant over-voltages may appear when a nonlinear load current has apparent specific harmonics [6]. This can also damage electrical equipment such as arresters, and greatly decrease the system reliability.

Therefore, it is necessary to improve the power quality in AC electric railway systems. Static var compensators (SVCs) and passive filters (PFs) are equipped in electric vehicles or traction substations (TSSs) [7]. However, those passive compensators have a large size, poor dynamic performance and so on. By overcoming these disadvantages, active power filters (APFs) and static synchronous compensators (STATCOMs) have effective roles in reactive and harmonic current elimination with a fast response, high efficiency, and low harmonic output [8]. The authors of [9] proposed a 6 MVA APF including a multiple-winding transformer. The authors of [10] proposed a hybrid APF (HAPF) improving the dynamic compensation performance, but the power switching devices usually suffer from a huge voltage stress. The authors of [11] presented a HAPF, but with a complex system design process. The authors of [12], [13] presented hybrid power quality compensators (HPQCs) that are connected to the point of common coupling (PCC) through a step-down transformer or a capacitive coupled branch, which may cause some adverse effect such as magnetic saturation, obvious temperature rise, huge space loss, or limits on fundamental power flow.

Cascaded H-bridge multilevel converters can be connected to the power supply directly without a step-down transformer or coupled branch, especially in STATCOM applications

Manuscript received Oct. 13, 2016; accepted Feb. 13, 2017
Recommended for publication by Associate Editor Saad Mekhilef.
†Corresponding Author: mlwu@bjtu.edu.cn
Tel: +86-51687081, Fax: +82-51687081, Beijing Jiaotong University
*School of Electronic Eng., Beijing Jiaotong University, China

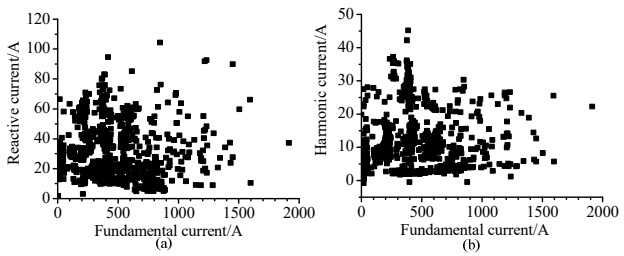

Fig. 1. Statistics of the reactive current and harmonic current characteristics.

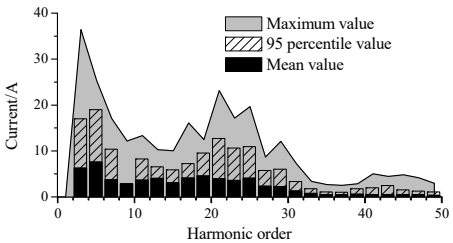

Fig. 2. Statistic of the harmonic currents.

[14]. Therefore, in this paper, a single-phase APF, with a cascaded H-bridge topology, is proposed to suppress the undesired reactive power and harmonic currents in AC electric railway systems. According to some field measured data in a TSS, the control strategy of a cascaded H-bridge multilevel APF is proposed and the control parameters are properly designed according to the converter topology and the desired compensation performance.

II. Traction Load Characteristics

Traction loads typically have time-varying and nonlinear features, and different types of electric vehicles have different load characteristics [15] that are decided by many factors such as the kinds of traction loads, load levels, line conditions, drivers' operation habits and so on. Therefore, large-scale actual data is useful, and statistical results can directly reveal the load characteristics for a specific TSS.

Field measured data is obtained in an electric railway TSSs for 24 hours. Some statistic characteristics of the traction load have been extracted. For example, Fig. 1 reveals the reactive current and total harmonic current, while Fig. 2 shows the maximum value, the 95 percentile value [16], and mean value of different harmonic currents. In this paper, the field measured data can offer basic reference information for APF design. This design method can optimize the parameters, improve the capacity utilization, and meet the power quality evaluation standards with the statistics field measured data. Although the levels of reactive power and harmonics have some differences in different TSSs, the design method and field measured data can provide some guidance for other APF designs.

III. System Configuration

A. Main Circuit Structure

In TSS, where the power quality has to be improved, one proposed APF is installed at each traction busbar, as shown in Fig. 3. The cascaded H-bridge multilevel converter is connected to a 27.5-kV power supply through a link reactor (L). In order to decrease the huge charging current, a charging resistor (R_{pre}) is included that connects a breaker (KM2) in parallel.

The cascaded H-bridge multilevel converter consists of n H-bridge cells, and each cell has the same structure and parameters. This topology can enlarge the converter rating and reduce the power device voltage stress without a transformer or resonance branch.

B. Parameters of the Main Circuit

Some of the main system parameters are analyzed in this section. The reactive and harmonic currents can be obtained according to the field measured data. In addition, the APF output voltage U_o should meet the requirement expressed in (1). The output voltage is the sum of the output voltages

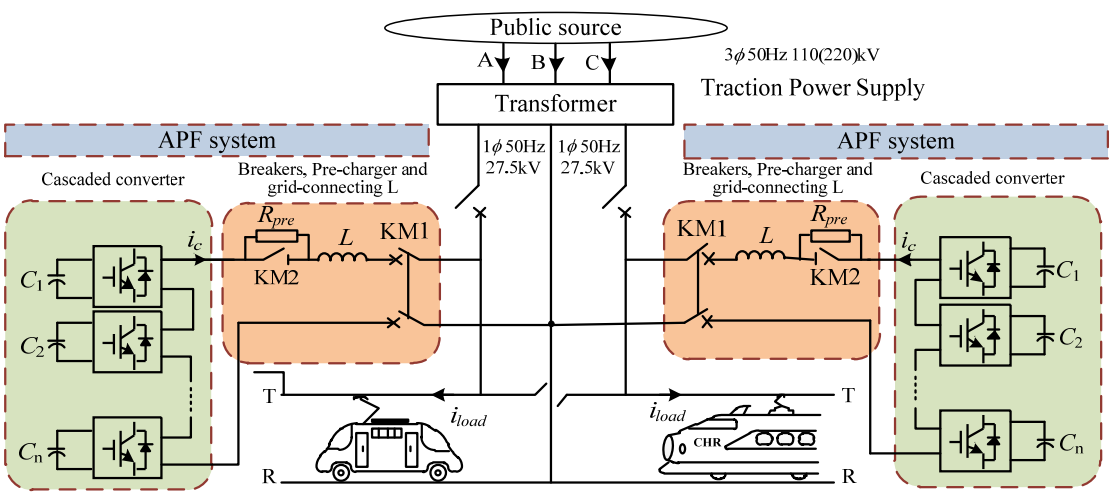

Fig. 3. Configuration of the proposed APF system.

of different H-bridge cells and it should be larger than the supply voltage in order to obtain enough current emitting capacity and good compensation performance, as expressed in (2) and (3).

$$U_o \geq \sqrt{U_{o\_f}^2 + U_{o\_h}^2} = \sqrt{(\omega L I_{Lq})^2 + \sum_{k=2}^{\infty}(k\omega L I_{Lk})^2} \quad (1)$$

$$U_o = nU_{dc}M/\sqrt{2} \leq nU_{dc}/\sqrt{2} \quad (2)$$

$$U_{dc} > \sqrt{2}U_s/n \quad (3)$$

where U_o is the RMS value of the APF output voltage, U_{o_f} and U_{o_h} are its fundamental and harmonic components, respectively, k is the harmonic order, I_{Lq} and I_{Lk} are the load reactive current and the k-th harmonic current, respectively, ω is the supply voltage angle frequency, n is the number of the H-bridge cells, and M is the amplitude modulation index.

Considering the voltage ratings of traditional power switching devices, a 3.3 kV - 400 A IGBT (Insulated Gate Bipolar Transistor) is designed as the power devices, and the DC-link voltage reference of the H-bridge cells can be set as U_{dc} = 1800 V in the proposed APF system. According to (1) - (3) and the field measured data, the number of the cells n can be estimated assuming the capacity utilization k_{dc} = 0.85. Considering the redundancy of the two H-bridge cells, the number of the cells can be obtained as n = 28.

$$n \geq \frac{\sqrt{2}U_s}{k_{dc}U_{dc}} = \frac{\sqrt{2}\times 27500}{0.85\times 1800} \approx 25.4 \quad (4)$$

The system compensation capacity of the proposed APF can be derived according to the rated supply voltage and the rated APF output current. In general, the maximum load harmonic current is used to obtain the compensation capacity for most traditional APFs [17]. However the stochastic volatility of the traction load and the large rating level are obvious. In order to make the full use of the compensation capacity, the 95 percentile values [18] of the field measured data can be used in the proposed APF system. Therefore, the capacity can be expressed as:

$$S = K_s U_s \sqrt{I_{Lq}^2 + \sum_{k=2}^{\infty} I_{Lk}^2} \quad (5)$$

where K_s (1.1~1.2) is the overload factor, and I_{Lq} and I_{Lk} are the 95 percentile values of the load reactive current and the k-th harmonic current, respectively.

IV. Control System

An overall block diagram of the APF control structure is designed with the dual-loop structure as shown in Fig. 4. It realizes some control functions such as: 1) the overall DC-link voltage control, which regulates the average DC-link voltage by controlling the active power exchange with the source; 2) the current reference tracking control, which consists of the active current, reactive current and harmonic current tracking control; and 3) the DC-link voltage balancing control, which keeps the capacitor voltages balanced.

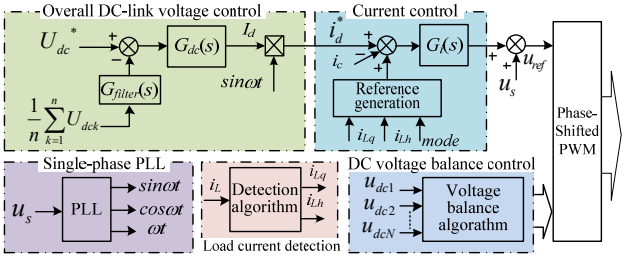

Fig. 4. Control system of the proposed APF.

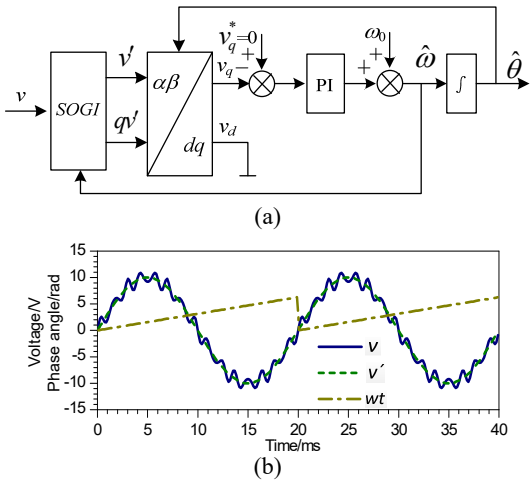

Fig. 5. Improved PLL based on a SOGI: (a) PLL structure, (b) PLL performance.

A. Suppression of Voltage Harmonics Influence

The proposed control algorithm needs a phase-locked loop (PLL) to obtain the phase angle of the supply voltage. However, the supply voltage usually contains some harmonics which limit the robustness and effectiveness of the conventional PLL. In order to eliminate the adverse impact of voltage harmonics, the authors of [19] presented an improved single-phase PLL based on a second-order generalized integrator (SOGI), and its structure and performance are shown in Fig. 5.

The performance of the improved PLL is affected by the parameters of the SOGI. A small gain coefficient k leads a good filtering effect, but a narrow bandwidth. On the other hand, a great gain coefficient k results in a good stability, because of the wide bandwidth. However, it also results in a weak filtering effect. In general, the supply voltage frequency may fall in the range of 49.8~50.2 Hz normally or 49.5~50.5 Hz when the power supply is weak. According to the performance and requirements of the expected PLL, the gain can be set to 1, and its amplitude and phase response are shown in Fig. 6. It can be seen that in the above frequency range, the amplitude gains are very close to 1 and the phase response errors are very small. Therefore, the proposed parameter is very reasonable in this application.

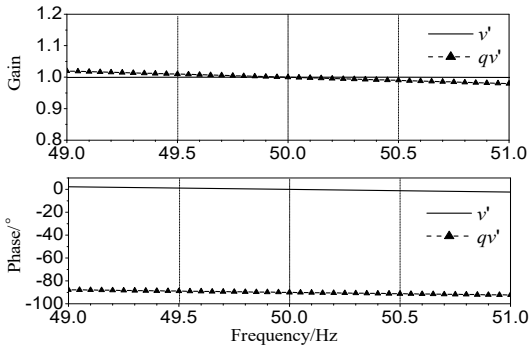

Fig. 6. Performance of the SOGI when k=1.

The supply voltage harmonics may result in extra harmonic currents which are undesirable and increase the burden for the APF. The supply voltage feedforward control is an effective method to eliminate the adverse influence of voltage harmonics, as shown in Fig. 4. This method is widely used, and this paper does not need to discuss it.

B. Overall DC-link Voltage Control and Filter

Since different H-bridge cells have the same demanded DC voltage reference, they share a common overall DC-link voltage control loop. A proportional integral (PI) controller is used and responsible for the capacitor voltage regulation to compensate the active power loss and to maintain a constant value, as shown in Fig. 4. The item of I_d is the controller output and the product i_d^* is the instantaneous value of the fundamental current reference.

Due to the input-output power balance feature for such a single-phase converter, a ripple voltage at twice the grid frequency is caused on the DC-link voltages, especially when delivering fundamental power. The ripple voltage can cause various problems depending on the application [20], such as leading a third-order harmonic current in the AC side. In order to suppress the undesired influences, a notch filter is used to eliminate the ripple voltage. The transfer function of the notch filter can be expressed as:

$$G_{noth}(s)=\frac{s^2+\omega_0^2}{s^2+\omega_0 s/Q+\omega_0^2} \tag{6}$$

where ω_0 is the characteristic angular frequency, and Q is the quality factor determining the bandwidth and gain.

In this application, the characteristic angular frequency is set to twice the grid frequency, $\omega_0 = 2\omega_n$. Different quality factor values lead different filtering performance, as shown in Fig. 7. The quality factor is selected as Q = 2.5 with a proper bandwidth and an enough gain.

C. Reactive and Harmonic Current Detection

There are many reactive current and harmonic current detection methods in single-phase systems [21], [22]. For example, the i_p-i_q method in a single-phase system is shown in Fig.8 (a). It draws DC components with a low-pass filter (LPF), and gets the harmonics by subtracting the fundamental

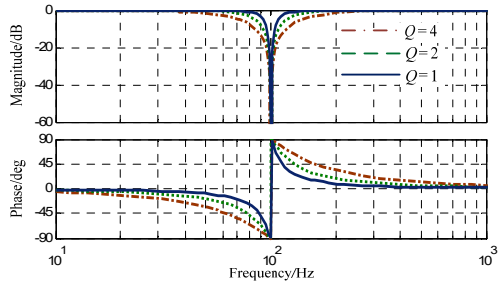

Fig. 7. Bode diagram of the notch filter.

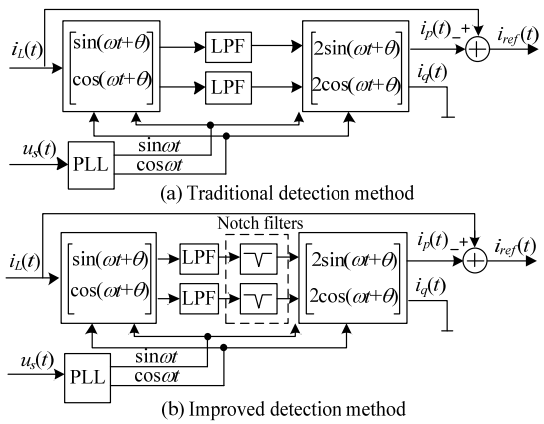

Fig. 8. Traditional and improved detection methods.

component from the total current. According to different reference currents, the APF can work in three different modes:

1) Reactive mode: the APF compensating the current reference is the detected reactive current, $i_{ref} = i_q$.

2) Harmonic mode: the current reference is the detected harmonic current, $i_{ref} = i_h = i_L - i_p - i_q$.

3) Comprehensive mode: the current reference is set to the sum of the load real-time reactive current and the harmonic current, $i_{ref} = i_q + i_h = i_L - i_p$.

However, the steady accuracy and response speed are usually not simultaneously satisfactory with the traditional LPFs in applications, such as with a fast response speed but second-order ripples on the output of the LPFs. The ripples can cause an obvious error in terms of the reactive current detection.

In this paper, notch filters are introduced to eliminate ripples, as exhibited in Fig. 8(b). Then the stable active and reactive current can be extracted, and the detected results are more accurate with a high response speed, as shown in Fig.9 and Fig. 10.

D. Current Tracking Control

1) Quasi Proportional-Resonant (QPR) Controller: As depicted in Fig. 4, the active component of the reference current i_d^* is generated through the overall DC-link voltage control loop. The total current reference is the sum of the active component i_d^* and the detected reactive and

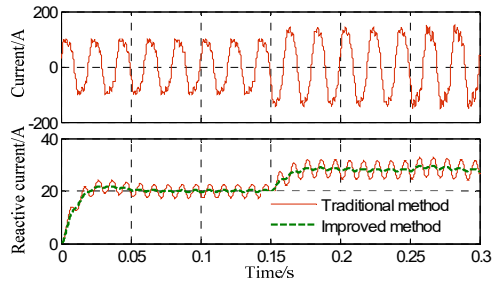

Fig. 9. Results of the reactive current detection.

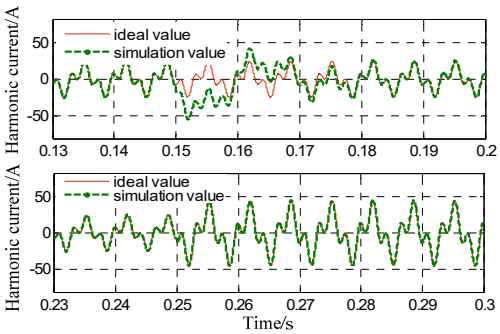

Fig. 10. Results of the harmonic current detection.

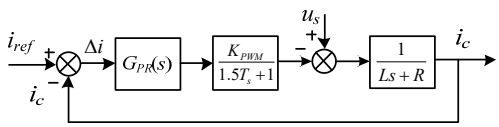

Fig. 11. Block diagram of the current control.

harmonic currents according to the operating mode. In this control system, a quasi proportional-resonant (QPR) controller [23] is adopted for the current reference tracking control. In addition, the transfer function of the controller is shown in (7). The generalized integrator (GI) component has a large gain at its resonant frequency ω_0. Therefore, the QPR controller can track sinusoidal references, such as the active and reactive current, with no phase or steady-state error [24]. The effect of the GI component can be neglected for the rest of the frequencies, and only the proportional gain K_p is considered when compensating harmonic currents.

$$G_{QPR}(s)=K_p+GI(s)=K_p+\frac{2K_r\omega_c s}{s^2+2\omega_c s+\omega_0^2} \tag{7}$$

where K_p is the proportional gain, K_r is the damping factor, ω_0 is the resonant frequency, and ω_c is the cutoff frequency.

The open-loop transfer function of the current loop involving the QPR controller and the closed-loop characteristic equation can be obtained in (8) and (9). Fig. 11 indicates a block diagram of the current loop.

$$G_o(s)=K\frac{s^2+2\omega_c\tau_i s+\omega_0^2}{\left(s^2+2\omega_c s+\omega_0^2\right)\left(1.5T_s s+1\right)\left(Ls+R\right)} \tag{8}$$

$$\left(s^2+2\omega_c s+\omega_0^2\right)\left(1.5T_s s+1\right)\left(Ls+R\right)+K\left(s^2+2\omega_c\tau_i s+\omega_0^2\right)=0 \tag{9}$$

where $K=K_{PWM}K_p$, $\tau_i=(1+K_r/K_p)$, and K_{PWM} is the converter equivalent gain.

2) Parameter Tuning: The parameters of the controller impact the stability and accuracy of the whole control system. Therefore, the control system requires proper parameters for the QPR controller to obtain a proper bandwidth for the current reference tracking.

For the fundamental current control, the resonant frequency of the QPR controller ω_0 can be kept the same as the supply voltage frequency ω_n ($\omega_0=\omega_n$). The parameter ω_c determines the bandwidth of the GI component. Assuming that the supply voltage frequency error ranges from -0.5 - 0.5 Hz [25], the bandwidth $2\omega_c$ should meet the requirement expressed in (10). Therefore, considering a certain margin, the resonant frequency ω_c can be obtained as ω_c= 5 rad/s.

$$2\omega_c>2\pi\times2\times0.5=2\pi \tag{10}$$

In order to obtain enough of an open-loop gain and to decrease the steady error, the gain at the resonant frequency is set to 60 dB, as (11) shown [26]. Furthermore (12) can be derived.

$$20\lg|G_{PR}(s)|_{s=j\omega 0}=60\ \text{dB} \tag{11}$$

$$K_p+K_r=1000 \tag{12}$$

For harmonic current control, the GI component and time delay of the control system can be neglected, and the closed-loop transfer function is obtained as:

$$G_{hcl}(s)=\frac{K_{PWM}K_p}{Ls+R+K_{PWM}K_p}=\frac{K}{Ls+R+K} \tag{13}$$

The bandwidth is $\omega_{bw}=2\pi f_{bw}=(R+K)/L$. It should be up to the largest harmonic current frequency and greatly below the switching frequency expressed in (14) (f_m=13×50 Hz, R=1 Ω, L=0.035 H, f_s=12800 Hz). Then the compensation performance is enough with a range of $K_p\in[142\sim307]$.

$$2\pi f_m<(R+K)/L<0.1\times2\pi f_s \tag{14}$$

The root-locus of (9) can be expressed in Fig. 12 with different K_p values. All of the root-locus locates in the left half plane and expresses the wide range of the stable operation area. The system can obtain a satisfactory performance when the roots stay in the range of *a* to *b* (or *c* to *d*), and this range is valuable in terms of the parameter design. Then K_p = 250 and K_r = 750 are used in the current loop after a lot of trial and error.

E. DC-link Voltage Balancing Control

Due to non-ideal converters and their different internal losses, the DC-link voltages of H-bridge cells have significant differences. The DC-link voltage imbalance can affect the compensation performance and even damage the power switching devices or lead to a complete collapse of the power-conversion system [27].

Many DC-link voltage balancing strategies have been proposed, such as adjusting the duty cycles [28], switching the redundant states [29], and switching the active vectors [30]. In this paper, introducing a balancing strategy based on adjusting the active vectors, and an additional control loop,

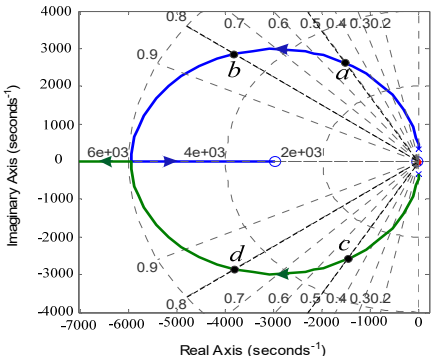

Fig. 12. Root-locus plot for the system characteristic equation.

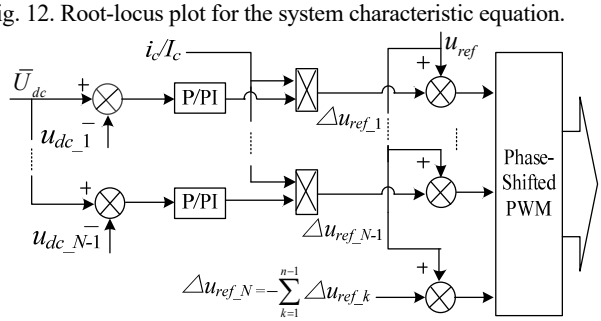

Fig. 13. Block diagram of the DC-link voltage balance control.

with a P (or PI) controller for each H-bridge cell, is used to achieve DC-link voltage balance control, as shown in Fig. 13.

The regulating variables lead an active power exchange between the AC source and the DC capacitors. Equation (15) shows the absorbed energy ΔE_{ac} caused by the regulating variable ΔU_{ref} in the AC side. The constant T_1 is the source fundamental voltage period. Assuming that the change of the DC-link voltage is ΔU_{dc}, (16) shows the energy change in the DC side. Considering the converter as a power lossless system, the DC-link voltage change can be obtained expressed in (17). Therefore, the individual balancing control loops can push the DC-link voltages to their average value and achieve balance control with proper regulating variables.

$$\Delta E_{ac}=\int_{t_0}^{t_0+T}M\Delta u_{ref}i_c dt=\int_{t_0}^{t_0+T}M\sum U_k\sin(k\omega t+\delta_k)\times \sum I_k\sin(k\omega t+\delta_k)dt=0.5MT_1\sum U_kI_k \tag{15}$$

$$\Delta E_{dc}=\frac{1}{2}C\left(U_{dc}+\Delta U_{dc}\right)^2-U_{dc}^2\approx CU_{dc}\Delta U_{dc} \tag{16}$$

$$\Delta U_{dc}=0.5MT_1\sum U_kI_k \tag{17}$$

If the P controller is executed in the DC-link voltage balancing control, in order to inhibit the obvious adverse impact on the compensation performance, the regulating variables can be limited by:

$$0.1U_{tri}<\gamma U_{dc}K_{P\_bal}K_{PWM}<0.5U_{tri} \tag{18}$$

where γ is the voltage fluctuation rate, U_{tri} is the carrier amplitude, and K_{P_bal} is the controller proportional coefficient.

This range is a result of trial and error, and it can offer an easy method and provide some guidance for parameter tuning:

TABLE I
MAIN SIMULATION PARAMETERS

Quantity	Value
Supply voltage	27.5 kV/50 Hz
Coupling inductance	35 mH
DC capacitor (H-bridge cell)	7650 F
IGBT switching frequency	500 Hz
Number of H-bridge cells	28
DC-link voltage	1800 V

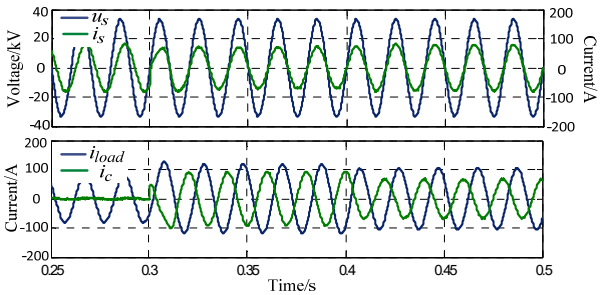

Fig. 14. Waveforms with a step load change in the reactive power compensation mode.

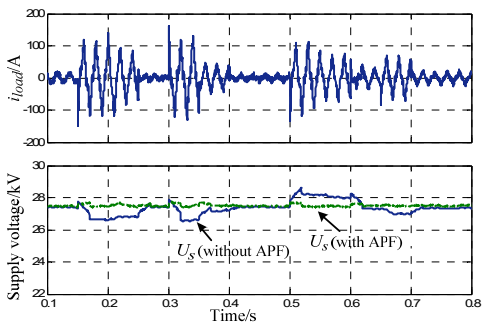

Fig. 15. Load current and traction busbar voltages.

$$\frac{0.1U_{tri}}{\gamma U_{dc}K_{PWM}}<K_{P\_bal}<\frac{0.5U_{tri}}{\gamma U_{dc}K_{PWM}} \tag{19}$$

V. SIMULATION AND EXPERIMENT RESULTS

A. Simulation Results

To verify the effects of the proposed cascaded H-bridge multilevel APF system, several simulations have been carried out using Matlab/Simulink. The main simulation parameters are presented in Table I. The power grid and traction transformer are described as a 27.5-kV voltage source.

Fig. 14 shows the results in the reactive mode, when the APF starts to operate at t=0.3 s and the traction load decreases at t=0.4 s. The output current i_c can reach a steady value in about 10 ms, which is a nice time response.

As a dynamic load, the change of the total reactive power of a trolley line can cause supply voltage (busbar voltage) fluctuations, especially in freight railroads. An APF can suppress undesirable fluctuations and maintain the stability of the supply voltage as Fig. 15 shown.

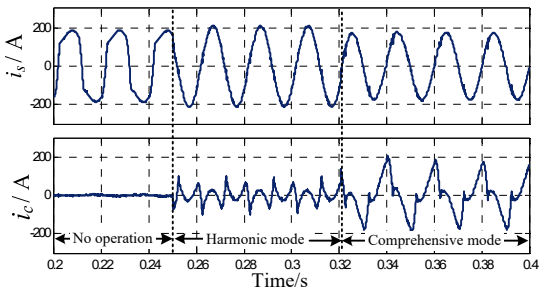

Fig. 16. Waveforms when changing the operation modes.

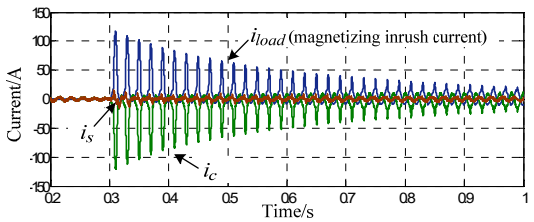

Fig. 17. Waveforms when compensating the magnetizing inrush current.

A nonlinear load is applied in the simulation model, and Fig. 16 shows the results of the APF operating in the harmonic mode and in the comprehensive model. The APF can operate in different modes with good stable and dynamic performances.

The magnetizing inrush currents of locomotive transformers are load transient fluctuations, containing reactive and harmonic current. An APF can offer transient current instead of the TSS to eliminate the adverse impact on the source current, as shown in Fig. 17.

B. Experimental Results

An experimental prototype of the proposed APF based on a cascaded H-bridge multilevel (5 H-bridge cells, 11 levels) converter has been implemented in the laboratory. Fig. 18 shows the laboratory prototype of the APF.

The carrier phase-shifted PWM (CPS-PWM) method is used to generate driving signals for the power switching devices. Fig. 19(a) and (b) reveal the output voltages of different H-bridge cells and the cascaded converter output voltage without any load. The H-bridge output voltages are phased-shifted to generate a multilevel voltage waveform. The results verify the performance of the CPS-PWM technology.

Reactive and nonlinear loads are connected to the source in Fig. 20 (a) and Fig. 20 (b), respectively. The source current is forced to be in phase with the supply voltage in different load conditions, and the source current distortion is decreased. Experiment steady results verify the basic reactive power compensation and harmonic current elimination performance.

Fig. 21 shows transient waveforms when the APF starts to operate, the load has a step change and in different modes. A new stability operating state can be quickly achieved in these transient processes. The fast response contributes to a nice

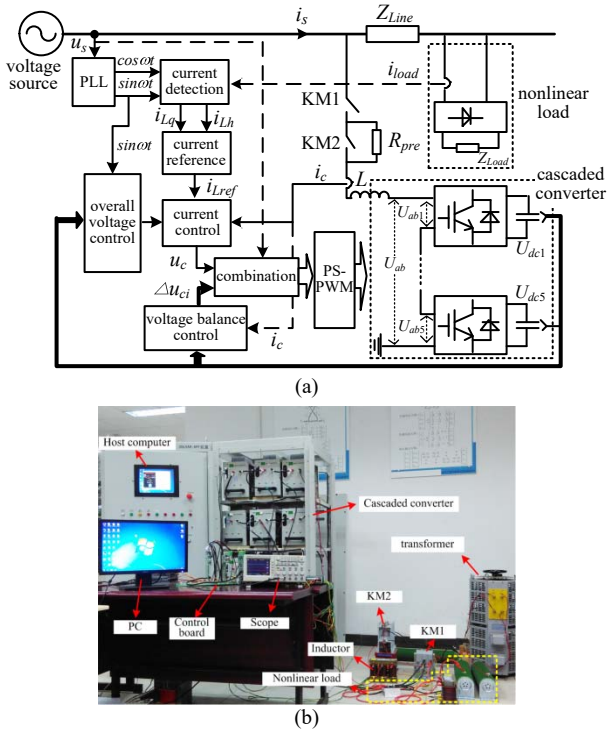

Fig. 18. Laboratory prototype of the APF. (a) Experimental schematic diagram. (b) Experimental APF circuit.

transient compensation performance. In addition, the notch filter in the overall DC-link voltage loop inhibits the 3-rd harmonic current in the AC side, and Fig. 22 shows the experimental results.

The supply voltage provided by the secondary winding of the laboratory regulating transformer is 125 V. The different inductive loads are fed by the source at different times, and they can be regard as locomotives running on the railway line, as shown in Fig. 23(a). Massive reactive power, produced by loads, causes supply voltage drops (0.12 pu), and these drops can be effectively suppressed (0.024 pu) with the APF, as shown in Fig. 23(b).

The switching-on process of a locomotive transformer without a load may result in a huge magnetizing inrush current. A load with a saturable transformer produces an obvious magnetizing inrush current, and Fig. 24 shows the experimental result with the APF. It shows that the APF offers the most transient current, leading to only very small source current fluctuations. Therefore, the APF can contribute to eliminating some of the source current transient fluctuations.

The DC-link voltage balancing control method mentioned in Section IV is used for the experimental prototype. In addition, the DC voltages of the first and third H-bridge cells U_{dc1} and U_{dc3} are picked up to display the balancing control performance in different conditions, and Fig. 25 shows the experimental results. The DC-link voltages can reach balanced operation with different initial voltage errors as

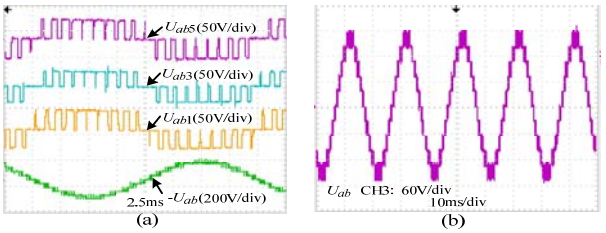

Fig. 19. Output voltages of the H-bridges and cascaded converter.

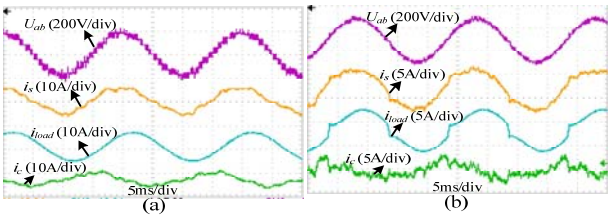

Fig. 20. Waveforms of steady-state experiment results: (a) with a reactive load, (b) with a nonlinear load.

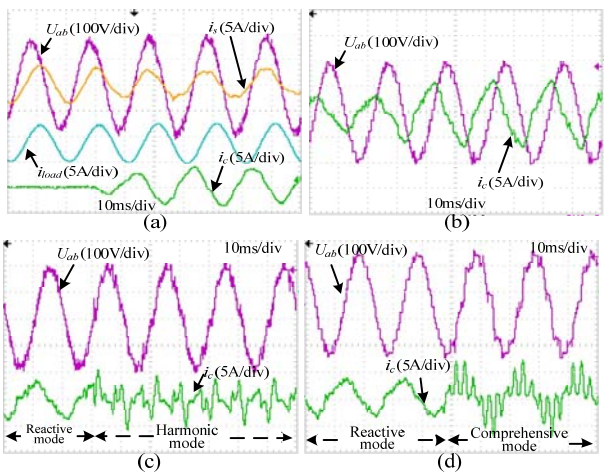

Fig. 21. Transient experimental waveforms: (a) when the APF starts to operate, (b) under load step change, (c) and (d) during different modes.

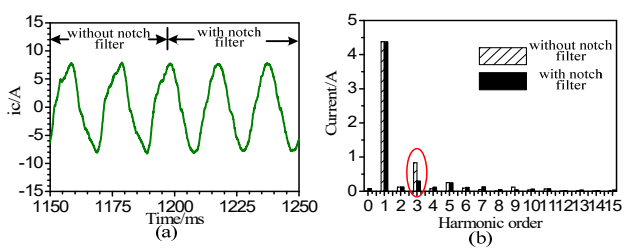

Fig. 22. Performance with and without a notch filter: (a) compensating current, (b) harmonic spectrum.

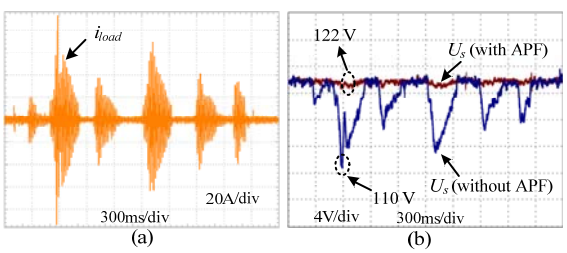

Fig. 23. Supply voltage RMS values with some load fluctuations: (a) load current, (b) supply voltages with and without the APF.

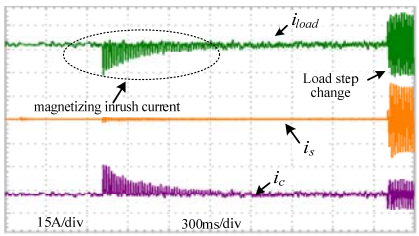

Fig. 24. Waveforms when the load produces a magnetizing inrush current.

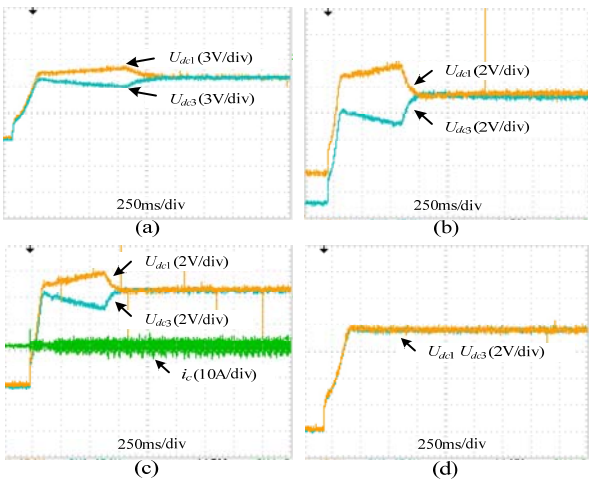

Fig. 25. Experimental results of the DC-link voltage balance control under different conditions.

shown in Fig. 25(a)-(d). In particular, it can obtain a nice balance performance when starting the balancing algorithm at the beginning, as shown in Fig. 25(d). It can be shown that the DC-link balancing control is effective in cascaded H-bridge APF applications.

VI. Conclusions

In this paper, a cascaded multilevel H-bridge APF is proposed for reactive power compensation and harmonic current elimination in AC electric railway systems. The traction load characteristics are analyzed based on field measured data at a Chinese electric railway TSS for the proposed APF design. The control strategy is analyzed and shown to achieve admirable stable and dynamic performance. Considering some problems, such as supply voltage fluctuations and transient inrush current, simulation and experimental results verify the feasibility of the power quality improvement in AC electric railway systems.

Acknowledgment

The authors wish to acknowledge the financial supports from the *Fundamental Research Funds for the Central Universities* of China (under grant 2015YJS157).

References

[1] G. Lin, X. Yonghai, X. Xiaoning, J. Peisi, and Z. Yunyan,

"Simulation model and harmonic analysis of SS6b electric locomotive based on PSCAD/EMTDC," in *Proc. EPEC*, pp.1-5,2008

[2] P. Caramia, G. Carpinelli, P. Varilone, P. Verde, D. Gallo, and R. Langella, "High speed AC locomotives: harmonic and inter harmonic analysis at a vehicle test room," in *Proc. IEEE Harmonics and Quality of Power*, pp. 347-353, 2000.

[3] G. Lin, X. Yonghai, X. Xiaoning, L. Yingying, and J. Peisi, "Analysis of adverse effects on the public power grid brought by traction power supply system," in *Proc. IEEE Elect. Power Energy Conference*, pp. 1-7, 2008.

[4] S. Zeliang, X. Shaodeng, and L. Qunzhan, "Single-Phase Back-To-Back Converter for Active Power Balancing, Reactive Power Compensation, and Harmonic Filtering in Traction Power System," *IEEE Trans. Power Electron.*, Vol. 26, No. 2, pp. 334-343, Feb. 2011.

[5] P. C. Tan, P. C. Loh, and D. G. Holmes, "A robust multilevel hybrid compensation system for 25-kV electrified railway applications," *IEEE Trans. Power Electron.*, Vol. 19, No. 4, pp. 1043-1052, Jul. 2004.

[6] Z. He, H. Hu, Y. Zhang, and S. Gao, "Harmonic resonance assessment to traction power-supply system considering train model in china high-speed railway," *IEEE Trans. Power Del.*, Vol. 29, No. 4, pp. 1735-1743, Aug. 2014.

[7] Z. He, H. Haitao, and G. Shibin, "Passive Filter Design for China High-Speed Railway With Considering Harmonic Resonance and Characteristic Harmonics," *IEEE Trans. Power Del.*, Vol. 30, No. 1, pp. 505-514, Feb. 2015.

[8] H. Junfei, L. Zhang, and S. J. Watkins, "Active power filtering by a flying-capacitor multilevel inverter with capacitor voltage balance," in *Proc. IEEE International Industrial Electronics*, pp. 2348-2352, 2008.

[9] K. M. Kwon, Y. S. Song, and J. Choi, "6MVA single-phase APF for high speed train line in Korea," in *Proc. IEEE Power Engineering and Renewable Energy*, pp.31-36, 2014.

[10] H. Park, J. Han, and J. Song, "Control Strategy for Shunt Active Power Filter Using Hybrid Multi-level Inverter in AC Electrified Railway Systems," *IETE Journal of Research*, Vol. 58, No. 6, pp.451-458, Jul. 2012.

[11] Z. Wang, J. Wang, J. Liu, J. Wang, and G. Li, "Harmonic suppression in electric traction system based on a single-phase hybrid active filter," in *Proc. IET Sustainable Power Generation and Supply*, pp.1-5, 2012.

[12] N. Y. Dai, K. W. Lao, M. C. Wong, and C. K. Wong, "Hybrid power quality conditioner for co-phase power supply system in electrified railway," *IET Power Electronics*, Vol. 5, No.7, pp.1084-1094, Aug. 2012.

[13] B. Chen, C. Zhang, C. Tian, J. Wang, and J. Yuan, "A hybrid electrical magnetic power quality compensation system with minimum active compensation capacity for V/V cophase railway power supply system," *IEEE Trans. Power Electron.*, Vol. 31, No. 6, pp.4159-4170, Sep. 2016.

[14] R. Xu, Y. Yu, R. Yang, G. Wang, D. Xu, B. Li, and S. Sui "A novel control method for transformerless H-bridge cascaded STATCOM with star configuration," *IEEE Trans. Power Electron.*, Vol. 30, No. 3, pp.1189-1202, Apr. 2015.

[15] S. M. M. Gazafrudi, A. T. Langerudy, E. F. Fuchs, K. Al-Haddad, "Power quality issues in railway electrification: a comprehensive perspective," *IEEE Trans. Ind. Electron.*, Vol. 62, No. 5, pp.3081-3090, Dec. 2015.

[16] GB/T14549 93, Quality electric energy supply Harmonics public supply network, Chinese Std, 1993.

[17] N. Zhou, J. Wang, Q. Wang, N. Wei, and X. Lou, "Capacity calculation of shunt active power filters for electric vehicle charging stations based on harmonic parameter estimation and analytical modeling," *Energies*, Vol. 7, No. 8, pp. 5425-5443, Aug. 2014.

[18] L. Qionglin, W. Bifang, and H. Yuhang, "Optimal compensation capacity design for active power filters in considering harmonics stochastic characteristics," *Automation of Electric Power Systems*(in Chinese), Vol. 31, No. 15, pp. 61-64 +93, Aug. 2007.

[19] S. Golestan, M. monfared, F. D. Freijedo, and J. M. Guerrero "Dynamics assessment of advanced single-phase pll structures," *IEEE Trans. Ind. Electron.*, Vol. 60, No. 6, pp. 2167-2177, Jun. 2013.

[20] H. Li, K. Zhang, H. Zhao, S. Fan, and J. Xiong "Active power decoupling for high-power single-phase pwm rectifiers," *IEEE Trans. Power Electron.*, Vol. 28, No. 3, pp.1308-1319, Jul. 2013.

[21] W. Jianmin, Z. Guo, Z. Xiaomin, and T. Mengmeng, "Several methods to improve the accuracy of adaptive harmonic current detection for single-phase circuits," in *Proc. ICEMI*, pp.316-320, 2013.

[22] W. Li Ran and W. Mingli, "Detection method for single-phase random harmonic current without PLL," *Applied Mechanics & Materials*. Vol. 719-720, No. 5, pp.622-629, Jan. 2015.

[23] R. Teodorescu, F. Blaabjerg, M. Loserre, and P. C. Loh, "Proportional-resonant controllers and filters for grid-connected voltage-source converters," *IEE Proceedings-Electric Power Applications*, Vol. 153, No.5, pp.750-762, Sep. 2006.

[24] R. Pena-Alzola, M. A. Bianchi, and M. Ordonez, "Control design of a PFC with harmonic mitigation function for small hybrid AC/DC buildings," *IEEE Trans. Power Electron.*, Vol. 31, No. 9, pp. 6607-6620, Nov. 2016.

[25] W. Na, M. Yuanpeng, "Harmonic current elimination for rectifiers based on *N* Times notch filter and PR controller," *Electric Drive for Locomotives* (in Chinese), Vol.2, No. 1, pp. 61-66, Mar. 2015.

[26] X. Hailiang, L. Zili, H. Yikang, "Key points of proportion-resonant controller applied for pwm converters," *Automation of Electric Power Systems* (in Chinese), Vol.18, No.1, Sep. 2015.

[27] Y. Xingwu, J. Jiang, and S. Liu, "A novel design approach of DC voltage balancing controller for cascaded h-bridge converter-based STATCOM," in *Proc. IEEE Power Electronics and Motion Control*, pp.2359-2364, 2009.

[28] X. She, A. Q. Huang, T. Zhao, and G. Wang, "Coupling effect reduction of a voltage-balancing controller in single-phase cascaded multilevel converters," *IEEE Trans. Power Electron.*, Vol. 27, No. 8, pp. 3530-3543, Aug. 2012.

[29] M. Morteza, G. Farivar, H. Iman-Eini, and S. M. Shekarabi, "A voltage balancing strategy with extended operating region for cascaded H-bridge converters," *IEEE Trans. Power Electron.*, Vol. 29, No,9, pp.5044-5053, Sep. 2014.

[30] Z. Liu, B. Liu, S. Duan, and Y. Kang, "A novel DC capacitor voltage balance control method for cascade multilevel STATCOM," *IEEE Trans. Power Electron.*, Vol. 27, No.1, pp. 14-27, Jan. 2012.

Liran Wu received his B.S. degree in Electrical Engineering from Yanshan University, Qinhuangdao, China. He is presently working towards his Ph.D. degree in the Department of Electrical Engineering, Institute of Traction Power Supply, Beijing, China. His current research interests include harmonic analysis in traction power supply systems, traction converters, high-voltage and high-power converters, and cascaded active power filter topologies and control.

Mingli Wu (M'76–SM'81–F'87) was born in Hebei, China, on November 11, 1971. He received his B.S. and M.S. degrees in Electrical Engineering from Southwest Jiaotong University, Chengdu, China, in 1993 and 1996, respectively; and his Ph.D. degree in Electrical Engineering form Beijing Jiaotong University, Beijing, China, in 2006. Since 2008, he has been a Professor in the School of Electrical Engineering, Beijing Jiaotong Uiversity. His current research interests include power supplies for electric railways, the digital simulation of power systems and electric power quality.